DOI: 10.1021/ma100472r

Macromolecules
ARTICLE

Unique Tackification Behavior of Needle-like Sepiolite Nanoclay in Brominated Isobutylene-*co*-*p*-methylstyrene (BIMS) Rubber

K. Dinesh Kumar,[†] Andy H. Tsou,[‡] and Anil K. Bhowmick*,[†,§]

[†]*Rubber Technology Centre, Indian Institute of Technology, Kharagpur 721302, India, and*
[‡]*Corporate Strategic Research, ExxonMobil Research and Engineering, Annandale, New Jersey 08801.*
[§]*Present address: Indian Institute of Technology, Patna 800013, India*

Received November 15, 2009; Revised Manuscript Received April 3, 2010

ABSTRACT: Adhesion between two unvulcanized rubber surfaces of the same material is termed autohesive tack. Interdiffusion of polymer chains that takes place across the interface and their bulk properties controls the strength of the interface. In this work, for the first time, we have studied the influence of sepiolite nanoclay on the autohesive tack strength of brominated isobutylene-*co*-*p*-methylstyrene (BIMS) rubber. The tack strength of BIMS rubber dramatically increases with nanoclay concentration. For example, the tack strength of 8 phr of nanoclay loaded sample is nearly 300% higher than the tack strength of neat BIMS rubber. Various tack governing factors such as green strength, creep compliance, entanglement molecular weight, relaxation times, self-diffusion coefficient, average penetration depth of rubber chains, and monomer friction coefficient have been analyzed. The addition of nanoclay reduces the extent of molecular diffusion across the interface by reducing the chain mobility; however, the diffusion level is still sufficient to form entanglements on either side of the interface. The entanglements arising from the diffused chains of the nanocomposite samples show greater resistance to separation due to an increase in cohesive strength, onset of transition zone relaxation time, and monomer friction coefficient value of the BIMS rubber matrix by the nanoclay reinforcement. On the other hand, the diffused chains of the unfilled sample exhibit facile chain separation due to the less cohesive strength of the BIMS rubber matrix.

1. Introduction

Autohesive tack of elastomers is the ability of two unvulcanized elastomer surfaces of the same material to resist separation after they are brought into contact for a short period under light pressure.[1−5] When two rubber surfaces are joined above their glass transition temperature, distinct macroscopic interface between the joining pieces slowly disappears with time, and the mechanical strength of the interface progressively increases.[1] Disappearance of interface is primarily due to the diffusion of polymer chains from both sides across the interface.[3]

The most commonly accepted mechanisms for forming adhesive bonds are (i) adsorption, (ii) molecular interdiffusion, (iii) electrostatic interactions, and (iv) mechanical interlocking.[3] The primary mechanisms for the bond formation between two unvulcanized rubber surfaces are adsorption and molecular interdiffusion.[3] It has been reported earlier[4] that the following conditions must be met by a rubber compound for exhibiting high autohesive tack: (a) the two rubber surfaces must come into intimate molecular contact, (b) diffusion of polymer chains across the interface must take place, and (c) the bonds thus formed must be capable of resisting high stress before rupture. The first two conditions describe the bond formation and take place in series; i.e., the molecular contact always precedes interdiffusion of chain segments.[4]

In the rubber industry, autohesion or autohesive tack or self-adhesion is particularly necessary in the case of tire manufacture, where various parts, including the impermeable inner lining, the reinforced carcass, and the tread, usually made of different polymers, have to hold together until the tire is cured.[4,5]

*Corresponding author: Tel (91-3222) 283180, (91-612) 2277380; Fax (91-3222)-220312; e-mail anilkb@rtc.iitkgp.ernet.in, director@iitp.ac.in.

Generally, plasticizers like oil facilitate molecular diffusion across the interface by diminishing the entanglement density of the rubber chains, but diluted, interdiffused rubber chains are more easily separated than the neat sample, and hence the tack strength reduces.[4−6] On the other hand, low molecular weight tackifying resins are added to synthetic elastomer compounds to enhance tack and to prevent tack decay.[4,6−8] Similar to the action of oil, tackifying resins also reduce the entanglement density of the base elastomer; however, the interdiffused chains diluted with tackifiers resist separation significantly more than those diluted with oil.[6,8]

In the literature, it has also been shown that addition of reinforcing fillers like carbon black can increase the tack strength of elastomers.[9−13] For example, addition of 40 phr of carbon black to natural rubber (NR) resulted in a significant increase in the tack strength of NR.[9] The increase in the tack strength of NR by the addition of carbon black has been attributed to an increase in cohesive strength due to filler reinforcement.[9] On the other hand, addition of carbon black to styrene−butadiene rubber (SBR) resulted in a significant reduction in the tack strength.[4] It has already been established that a typical SBR cannot readily achieve bond formation due to the unfavorable intrinsic characters of the elastomer such as molecular weight and viscosity.[10] The addition of filler further restricts the chain mobility, reducing the interfacial interactions leading to lower tack.[10] Therefore, it was concluded that the effect of carbon black addition on tack depends more on elastomers' ability to achieve bond formation, rather than its specific chemical nature.[4,11]

Over the past decade, nanoclays have been used as a potential reinforcing agent for various elastomers.[14−16] These nanoclays offer a wide array of property improvements at very low filler loadings, owing to the dispersion of few nanometers thick clay

 Published on Web 04/12/2010

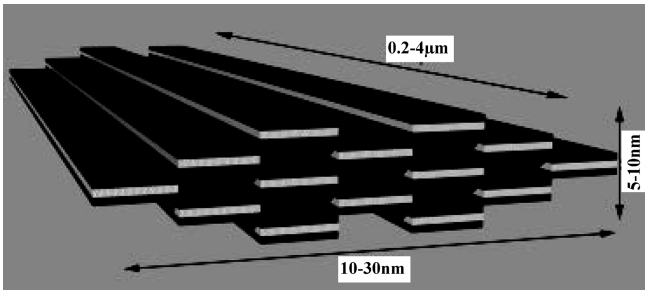

Figure 1. Schematic illustration of sepiolite nanoclay with characteristic average sizes, showing blocks and channels extending in the longitudinal direction. Each block is formed by two tetrahedral silica sheets and a central octahedral sheet containing Mg, represented by dark and light colors, respectively. More blocks are structurally linked to each other along their longitudinal edges by Si−O−Si bonds.[23]

platelets of high aspect ratio.[14] Research workers from our own group have extensively studied the effect of different platelet-like montmorillonite (MMT) nanoclays and needle-like sepiolite nanoclays on the physicomechanical properties of various elastomers.[16−22]

MMT nanoclay structure is made up of layers of two tetrahedrally coordinated silicon atoms fused to an edge-shared octahedral sheet of either aluminum or magnesium hydroxide.[16] The layer thickness is ∼1 nm, and the lateral dimensions of these layers vary from 30 to 100−150 nm.[16] These layers organize themselves into stacks leading to a regular van der Waals gap between the layers known as the interlayer or simply gallery gap.[14−16] Sepiolite is a hydrated magnesium silicate and is part of the phyllosilicate mineral family. It is formed of blocks structurally similar to layered clay minerals (i.e., montmorillonite), composed of two tetrahedral silica sheets and a central octahedral sheet containing Mg, but continuous only in one direction (*c*-axis) (see Figure 1).[23] More blocks are linked together along their longitudinal edges by Si−O−Si bonds, and this creates channels along the *c*-axis. Because of the discontinuity of the external silica sheets, a significant number of silanol groups (SiOH) are situated at the edges of this mineral. Sepiolite shows high surface areas, ∼200−300 m^2/g, due to its fine particle size and fibrous nature but also to the presence of channels and micropores. The dimensions of the fibers vary between 0.2−4 μm in length, 10− 30 nm in width, and 5−10 nm in thickness. Sepiolite is naturally found in bundles due to the attraction forces.[23] It is believed that this needle-like sepiolite nanoclay can be more easily dispersed in polymeric matrices because of its lower specific surface area when compared with the platelet-like clays of the same aspect ratio. The relatively small contact surface and hence the reduced tendencies to agglomerate could then lead to a better mechanical reinforcement of the needle-like clays.[20−22]

Most of the early efforts have been focused mainly to understand the influence of these nanoclays on the mechanical, thermal, and physical properties of various polymers.[14−16] Recently, self-assembling of polymers and nanoparticles into layers with controllable nanometer thickness useful in high end applications such as tandem solar cells, sensors, optical coatings, etc., is very popular within the polymer community.[24,25] On the other hand, much effort has not been focused to understand the effect of the nanoclays on the adhesive behavior of elastomers. There are only few reports in the literature that examine the effect of MMT-based nanoclays on the adhesive behavior of acrylic elastomer.[26,27] Very recently, Wang et al. have studied the effect of laponite nanoclay on the pressure-sensitive adhesive tack of acrylic adhesives measured by the probe tack technique.[28]

However, there has been no report on the effect of nanoclay the autohesive tack (self-adhesion) of any elastomer. Therefore, studying the effect of nanoclays at relatively very low concentrations on autohesive tack of elastomers is well justified. In the present study, we have studied the effect of sepiolite, needle-like nanoclay on the autohesive tack of brominated isobutylene-*co*-*p*-methylstyrene (BIMS) rubber with special regard to (a) nanoclay concentration, (b) morphology of rubber−clay nanocomposites, and (c) viscoelastic properties of rubber−clay nanocomposites. Additionally, the influence of sepiolite nanoclay concentration on the BIMS elastomer's bond formation (self-diffusion) and bond-breaking ability (strength of the interface) has been analyzed by studying various distinct tack governing parameters like green strength, creep compliance, entanglement molecular weight (M_e), relaxation times (τ), self-diffusion coefficient (D), average penetration depth of rubber chains (Δx) across the interface, and monomer friction coefficient (ζ_0).

Table 1. Composition of Mixes Prepared

sample no.	designation	BIMS rubber (g)	nanoclay (phr)[a]
1	B	100	0
2	BSEP2	100	2
3	BSEP4	100	4
4	BSEP8	100	8
5	BSEP16	100	16

[a] phr = parts per hundred grams of rubber.

2. Materials and Methods

2.1. Materials. Brominated isobutylene-*co*-*p*-methylstyrene, or BIMS (grade: Exxpro 3035; benzylic bromine of 0.47 ± 0.05 mol % and 2.0 mol % of *p*-methylstyrene, Mooney viscosity of 45 ± 5 at ML_{1+8} 125 °C and M_w = 450 000), was supplied by the ExxonMobil Chemical Co., Baytown, TX, and the sepiolite (grade: Pangel) was supplied by Tolsa, SA, Spain.

2.2. Preparation of Filled Samples. Mixes were prepared in a Brabender Plasticorder (model, PLE-330, capacity 65 mL, Duisburg, Germany) at 175 °C and 100 rpm. BIMS was taken in the Brabender mixer and sheared for 3 min. Then sepiolite nanoclay was added, and the mixing was continued for an additional 3 min. The neat BIMS rubber was also processed for 4 min under the same conditions. The composition of the mixes prepared is reported in Table 1.

2.3. Preparation of Test Samples. For determination of tack strength, rubber sheets (10 cm wide × 15 cm long × 2.5 mm thick) were prepared by pressing them at 150 °C for 5 min between smooth Mylar sheets at 5 MPa pressure in an electrically heated press (David Bridge, Castleton, England). One side of the rubber sheet was backed by a fabric about 1 mm thick. The samples were then left for 20 ± 2 h before testing for conditioning the samples. For the determination of maximum tensile stress, rubber sheets (10 cm wide × 15 cm long × 2.5 mm thick) were prepared by pressing them at 150 °C for 5 min between sheets of smooth aluminum foil at 5 MPa pressure in an electrically heated press. For studies on morphology and dynamic mechanical properties, rubber sheets (3 cm wide × 6 cm long × 1.5 mm thick) were prepared by pressing them at 150 °C for 5 min between sheets of smooth aluminum foil at 5 MPa pressure in an electrically heated press.

2.4. Morphology of Rubber Nanocomposites. *2.4.1. X-ray Diffraction (XRD) Studies.* For the characterization of the rubber nanocomposites, XRD studies were performed using a Philips X-PERT PRO diffractometer (The Netherlands) in the range of 2°−9° and Cu target (λ = 0.154 nm). Then, *d*-spacing of the clay particles was calculated using Bragg's law. The samples were placed vertically in front of the X-ray source. The detector was moving at an angle of 2θ, while the sample was moving at an angle of θ.

2.4.2. Atomic Force Microscope (AFM) Imaging. The morphology of nanocomposite samples was analyzed by AFM. AFM studies were carried out in air at ambient conditions

(25 °C, 60% RH) using multimode AFM from Veeco Digital Instruments, Santa Barbara, CA. Topographic phase images were recorded in the tapping mode atomic force microscopy (TMAFM) with the set point ratio of 0.9, using long tapping mode etched silicon probe (LTESP) tip having a spring constant in the range of 48 N/m. For each sample, a minimum of three images were analyzed. The cantilever was oscillated at a resonance frequency (ω_0) of ~280 kHz.

2.4.3. Transmission Electron Microscopy (TEM). The samples for TEM analysis were prepared by ultra-cryomicrotomy using a Leica Ultracut UCT. Freshly sharpened glass knives with cutting edge of 45° were used to get the cryosections of 50 nm thickness. Since these samples were elastomeric in nature, the sample temperature during ultra-cryomicrotomy was kept constant at −100 °C (which was well below glass transition temperature, T_g, of the BIMS rubber), at which the samples existed in hard glassy state, thus facilitating ultra-cryomicrotomy. The cryosections were collected and directly supported on a copper grid of 300-mesh size. The microscopy was performed later using a JEOL-2100 electron microscope (Japan), having a LaB_6 filament, operating at an accelerating voltage of 200 kV.

2.5. Contact Angle Measurements. The sessile drop method employing 2 μL drops of ethylene glycol probe liquid was applied on the surfaces of unfilled and filled samples for contact angle (θ) measurements in a contact angle meter (Kernco, Model G-II from Kernco Instruments, EI Paso, TX). Each contact angle quoted is the mean of at least five measurements with a maximum error in θ of ±1°. All investigations were carried in a vapor saturated air at 20 ± 2 °C in a closed sample box. The equilibrium was reached in 1 min, and no variation in θ was obtained thereafter. The advancing contact angle value of probe liquid at 5 min was recorded and reported in all cases.

2.6. Measurement of Tack Strength. In the present study, autohesive tack strength was measured by a 180° peel test. The schematic representation of autohesive tack strength measurement by a 180° peel test is shown in Figure 2. Previously, many researchers used the 180° peel test geometry for the estimation of autohesive tack strength.[6−8,12,13,29] Strips of (25.4 mm wide × 75 mm long × 2.5 mm thick) were cut from the previously prepared sheet. Mylar sheet was peeled just prior to testing. Tack testing was performed by placing two samples together with a Mylar insert at one end (contact area 25.4 mm × 55 mm). A load of 2 kg was applied in each case (~14.0 kN/m^2) by means of a specially designed handpress, with a provision for applying variable loads. After 15 s contact time, the average force required to separate the two strips was measured in a computerized Zwick/Roell Z010 (Zwick/Roell, Ulm, Germany) universal testing machine at 25 °C. The data were analyzed by testXpert II software of the Zwick/Roell universal testing machine. The tack strength G_a (N/m) was calculated using eq 1[7,8,12,13]

$$G_a = 2F/w \tag{1}$$

where F is the average force (N) required for peeling and w is the width (m) of the sample. For each system, four samples were tested, and the results were averaged. In order to optimize the peel rate, the samples were peeled at different rates (50, 100, 150, 200, and 250 mm/min) after 10 s contact time. At peel rates less than 250 mm/min, the rubber strips were in contact for longer time due to the slow peeling rate, and hence the nanoclay loaded samples could not be peeled (separation front was toward the rubber−fabric interface). At the optimized peel rate (i.e., at 250 mm/min), the contact time was also varied. However, the contact time could not be increased beyond 15 s. Therefore, the peel rate and contact time were kept as 250 mm/min and 15 s, respectively, for all the samples.

2.7. Measurement of Maximum Tensile Stress from Stress−Strain Curves. Green strength was estimated by measuring the maximum tensile stress from the stress−strain curves.[6−8] Maximum tensile stress measurement was done according to the ASTM D412-98T method. Dumbbell-shaped specimens were punched from the prepared sheets, and maximum tensile stress was measured in a computerized Zwick/Roell Z010 universal testing machine at 25 °C at a separation rate of 50 mm/min. The data were analyzed by testXpert II software of the Zwick/Roell universal testing machine. The maximum tensile stress was taken as the maximum stress in the stress−strain, $\sigma-\varepsilon$, curve. The tensile stress is defined as the ratio of the applied force to the initial, undeformed cross-sectional area, and the tensile strain is based on the initial sample length between the two grips. Four samples were tested for each system, and the average of the results was reported.

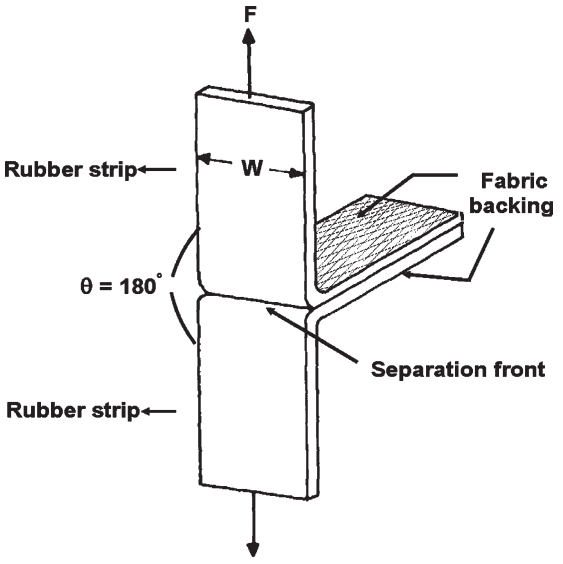

Figure 2. Schematic representation of autohesive tack measurement of elastomer by a 180° peel test geometry.

2.8. Determination of Viscoelastic Properties of Nanocomposites through Dynamic Mechanical Analyzer (DMA). *2.8.1. Creep Compliance Measurement.* The contact flow was measured by creep compliance measurements. The creep compliance tests were carried out in a dynamic mechanical analyzer (DMA Q 800 from TA Instruments, New Castle, DE) in tension mode geometry. In creep experiments, a constant stress, σ_0, of 0.025 MPa was imposed on the sample, and the resulting strain, ε, was measured as a function of time (t) at 25 °C. The sample dimensions were 6.25 mm wide × 30 mm long × 1.5 mm thick. From the stress and strain, the compliance $D(t)$ of the sample can be calculated by eq 2[30]

$$D(t) = \frac{\varepsilon(t)}{\sigma_0} \tag{2}$$

2.8.2. Temperature Sweep Test. Temperature sweep test was carried out in a dynamic mechanical analyzer (DMA Q 800 from TA Instruments) in tension mode geometry in the temperature range of −80 to 150 °C at a constant frequency of 1 Hz and at a constant strain of 0.1%. The sample dimensions were 6.25 mm wide × 30 mm long × 1.5 mm thick.

2.8.3. Frequency Sweep Test. The frequency sweep tests were carried out in a dynamic mechanical analyzer (DMA Q 800 from TA Instruments) in tension mode geometry. Measurements were made at 15 frequencies in the 0.01−25 Hz range at 0.1% strain and at different temperatures between −50 and 125 °C. All the results were reduced to 25 °C and shifted to form master curves by applying time−temperature superposition principle, and the results are presented as storage modulus, E', and loss modulus, E'', against frequency. The sample dimensions were 6.25 mm wide × 30 mm long × 1.5 mm thick.

3. Results and Discussion

3.1. Morphology of Nanocomposites. *3.1.1. X-ray Diffraction (XRD) Studies.* The X-ray diffractograms of the

pristine sepiolite nanoclay and BIMS−sepiolite nanocomposites are shown in Figure 3. The X-ray diffractogram of the pristine sepiolite nanoclay displays an intense peak around $2\theta = 7.2°-7.4°$ (d-spacing of 1.22−1.24 nm), corresponding to the internal channel reflections of the sepiolite needle-like structure.[22] After dispersion of the nanoclay in the BIMS matrix, the sepiolite internal channel diffraction peak is not shifted, attesting that the channel structure of the nanoclay particles remains unchanged (see Figure 3). This indicates that, unlike montmorillonite nanoclay which is a layered silicate, sepiolite clay does not undergo exfoliation on addition to the rubber matrix because the individual TOT (tetrahedral octahedral tetrahedral) layers of the sepiolite nanoclays are connected through covalent bond, and moreover the clay is also fibrous in nature.[22] From Figure 3, it is clearly seen that the peak intensity seems to be well correlated with the nanoclay content. Bhattacharya et al.[21] have predicted that the SBR chain can penetrate and reside in the long, narrow channels in the sepiolite clay structure, and under the shear forces experienced during melt mixing, the rubber chains drag away stacks of adsorbed clay by overcoming their cleavage energies. Considering the same hypothesis to be applicable here for BIMS−sepiolite clay nanocomposites, slight delamination of the clay layers under the high shear force cannot be ruled out. However, in order to have conclusive evidence regarding the dispersion of the sepiolite nanoclay in BIMS rubber, the surface morphology and bulk morphology of the nanocomposites have been studied through AFM and TEM, respectively. These results are discussed in the forthcoming sections.

3.1.2. Atomic Force Microscopy. AFM phase images of samples B, BSEP4, and BSEP8 are shown in Figure 4. The AFM phase image of sample B (Figure 4a) shows a very clean and smooth surface, which is perhaps due to the absence of nanoclay in sample B. On the other hand, the phase images of samples BSEP4 and BSEP8 (Figure 4b,c) show the presence of sepiolite needles all along the surface; some of them are associated but many prove to be individually spread over the surface, which seems to confirm some surface "nanostructuration". Some needles are lying on the surface (arrows). Individual points (circles) can be ascribed to sepiolite needles localized perpendicular to surface. In the literature, it has been reported that the size of the sepiolite nanoclay varies widely, but in most cases they are 10−5000 nm long, 10−30 nm wide, and 5−10 nm thick.[23,31] Here, the AFM phase image reveals that the average length, width, and thickness of the sepiolite needles are in the range of 400, 40, and 20 nm, respectively. This suggests a reasonably good dispersion of sepiolite nanoclay in BIMS surface. Also, some agglomerated clay particles having average thickness of about 60−120 nm are also seen in the AFM phase image of BSEP8.

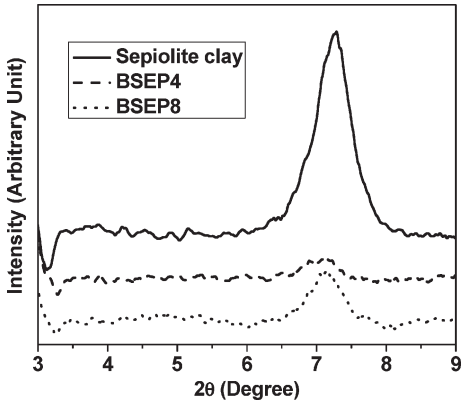

Figure 3. XRD patterns of pristine sepiolite nanoclay, BSEP4, and BSEP8.

3.1.3. Transmission Electron Microscopy. Since the AFM images show only the surface profile of the nanoclay/rubber mixtures, the TEM micrographs of the nanocomposites have been analyzed to understand the distribution of nanoclay particles in the bulk. However, while performing TEM analysis, the high TEM voltage resulted in degradation-induced deformation of the samples, and sometimes pictures could not be taken. Therefore, before performing TEM analysis, the unfilled and clay filled samples were mixed with 0.5 phr of *p*-phenylenediamine (PPD) antidegradant to prevent degradation of the samples. TEM micrographs of samples B, BSEP2, BSEP4, and BSEP8 are shown in Figure 5. As expected, the TEM micrograph of sample B (Figure 5a) does not depict any specific morphological pattern. The TEM micrographs of the filled samples (Figure 5b−d) confirm the uniform distribution of needle-like sepiolite nanoclay particles throughout the BIMS matrix. There is no evidence for the presence of bulk clay agglomeration even in sample BSEP8. Homogeneous "nano-structuration" of sepiolite nanoclay has been observed with regions filled with sepiolite nanoclay particles. The dimensions of the dispersed sepiolite nanoclay particles (length ~350−400 nm and width ~30−40 nm) observed from the TEM micrographs correlate well with the dimensions of the sepiolite nanoclay as observed in the AFM images (Figure 4b,c).

3.2. Effect of Nanoclay Concentration on Tack Strength of BIMS Rubber. The values of tack strength, G_a, of neat BIMS rubber (B−B) and BIMS−sepiolite nanoclay mixtures (BSEP2−BSEP2, BSEP4−BSEP4, and BSEP8−BSEP8) are shown in Figure 6. The tack strength of BIMS dramatically increases with increasing clay concentration. For example, the tack strength values of samples BSEP2 and BSEP8 are approximately 140% and 300% higher than the tack strength of sample B. At this juncture, it should be noted that the failure mode in the peel test for samples B, BSEP2,

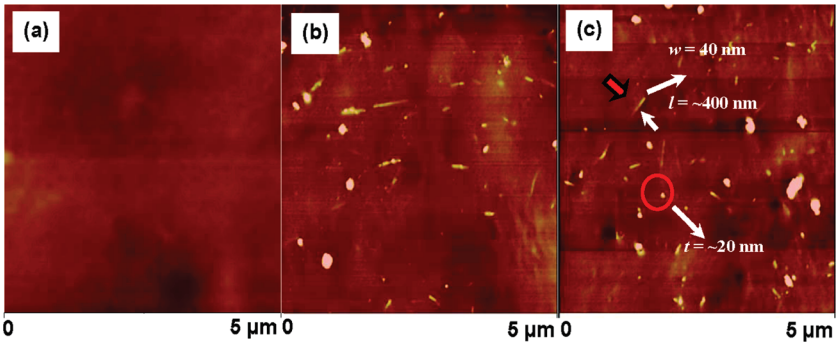

Figure 4. AFM phase images of (a) B, (b) BSEP4, and (c) BSEP8.

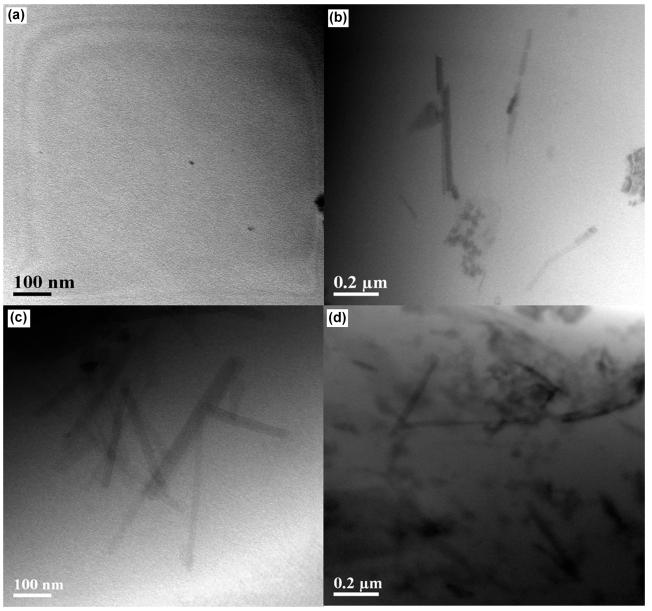

Figure 5. TEM micrographs of (a) B, (b) BSEP2, (c) BSEP4, and (d) BSEP8.

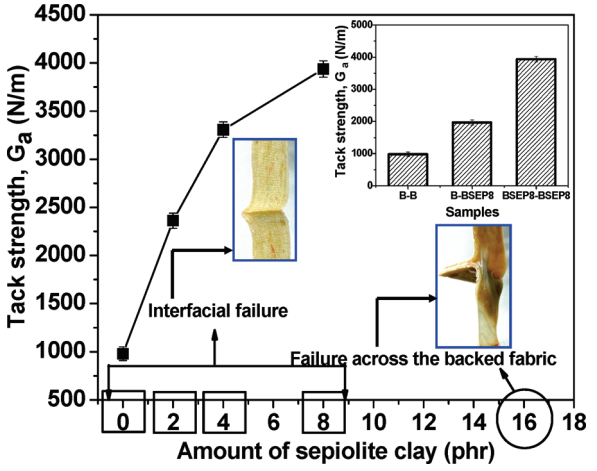

Figure 6. Effect of loading of nanoclay on autohesive tack strength of BIMS rubber and (inset) autohesive tack strength of B−B (joint strength between a strip of B and another strip of B), B−BSEP8 (joint strength between a strip of B and another strip of BSEP8), and BSEP8−BSEP8 (joint strength between a strip of BSEP8 and another strip of BSEP8).

BSEP4, and BSEP8 are interfacial type (see inset of Figure 6). However, at 16 phr of clay concentration, the failure mode in the peel test is cohesive type (failure along the backed fabric as shown in the inset of Figure 6). The force vs distance curves from the peel tests for selected samples are shown in Figure 7. For sample B, the separation front traveled exactly along the center plane of the test pieces, and therefore there is an initial peak followed by a nearly constant peel force with small, random fluctuations. The peel force, *F*, has been taken to be the average value, excluding the initial peak, as conventionally followed by other researchers for the measurement of autohesive tack strength by a 180° peel test geometry.[6,32] For 2, 4, and 8 phr nanoclay loaded samples, the separation front sometimes shifted from the center plane to the rubber/fabric interface and again proceeded along the center plane, and hence their failure patterns in the peel curves are different in comparison with the neat BIMS

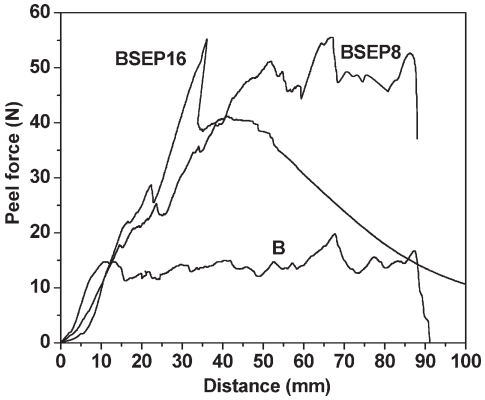

Figure 7. Peel force−distance curves for B, BSEP8, and BSEP16.

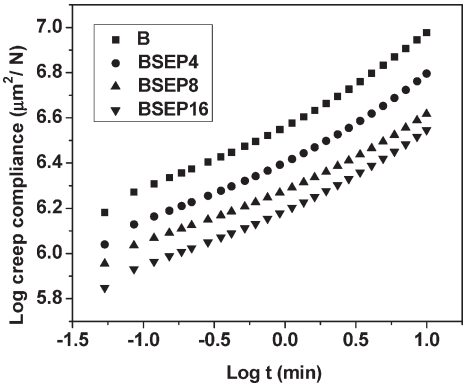

Figure 8. Creep compliance of B, BSEP4, BSEP8, and BSEP16.

rubber. However, even in these cases, peeling occurred along the center plane over a sufficient length to estimate the average peel force. In the case of sample BSEP16, the separation front shifted spontaneously from the center plane to the elastomer/fabric interface, and therefore peeling along the interface could not be made (Figure 6).

In the literature, it has been reported that addition of carbon black to SBR and EPDM lowers the tack strength as compared to that of gum elastomers.[4,10,11,33,34] However, BIMS shows a different behavior, which is similar to that observed for natural rubber.[4,9] Furthermore, Kumar et al. have reported that addition of large amount of (> 30 phr) carbon black and silica to BIMS rubber improves the autohesive tack strength of BIMS rubber.[12]

It is well-known that the addition of reinforcing fillers will increase the green strength of synthetic elastomers and can reduce the contact flow and extent of diffusing rubber molecules at the tack junction. If the reduction in contact flow dominates over the enhancement in green strength, there will be reduction in the tack strength. Here, the creep compliance (contact flow) of BIMS is reduced by the addition of nanoclay (Figure 8). In addition, the green strength of BIMS rubber is enhanced by the addition of nanoclay (Figure 9). The maximum tensile stress of BIMS rubber gradually increases (from 0.25 to 0.32 MPa at 16 phr nanoclay concentration) with increasing loading of nanoclay (Figure 9).

The reduction in contact flow and enhancement in green strength of BIMS rubber by the addition nanoclay can be ascribed to the reinforcing action of the nanoclay in the BIMS matrix. In spite of reduction in the contact flow by the addition of nanoclay, the tack strength of BIMS dramatically increases. Therefore, in the case of the BIMS−sepiolite

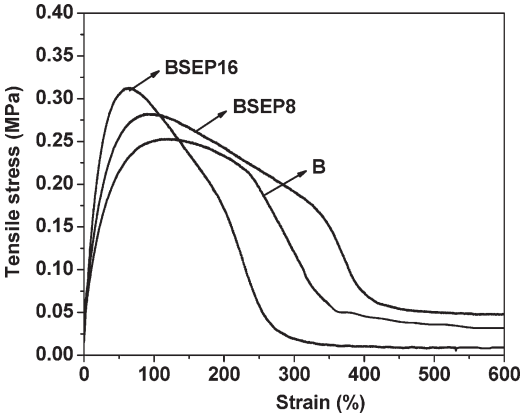

Figure 9. Tensile stress vs strain plots of B, BSEP8, and BSEP16.

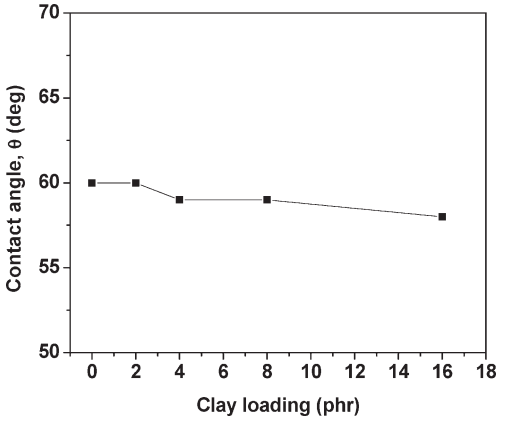

Figure 10. Contact angle of ethylene glycol at 25 °C on B, BSEP2, BSEP4, BSEP8, and BSEP16.

system, it may be derived that the increase in green strength dominates over the decrease in contact flow. The drop in contact flow must be low, and it should be still sufficient to establish interdiffusion and entanglements across the interface. In addition, the entangled chains in the clay loaded samples should show higher resistance to separation upon stressing due to the higher monomer friction coefficient value in the clay loaded samples when compared to neat BIMS rubber. The monomer friction coefficient and self-diffusion coefficient values of the unfilled and clay loaded samples have been calculated from the DMA frequency sweep master curves, and these results are discussed in detail in a later section.

Next, we consider the other main features in the tensile stress−strain ($\sigma-\varepsilon$) curves (Figure 9). It is very instructive to determine how changes in the $\sigma-\varepsilon$ curves might affect autohesion.[8] Figure 9 shows that the addition of nanoclay stiffens the rubber (increases Young's modulus). The increase in the elastic modulus (determined at low strain) of BIMS rubber with the concentration of nanoclay elucidates the reinforcing action of nanoclay. In addition, incorporation of 8 phr of nanoclay (BSEP8) increases the area under the $\sigma-\varepsilon$ curve by concomitantly increasing the maximum tensile stress and the percentage elongation. This suggests the potential of BSEP8 to dissipate a greater amount of energy before failure when compared to B, and hence the tack strength of BSEP8 is higher than the tack strength B. However, at 16 phr of nanoclay loading (BSEP16), there is decrease in the area under the $\sigma-\varepsilon$ curve, which is perhaps due to the good chance of aggregation of nanoclay particles at higher concentration. It is well-known from the existing literature that in order to achieve high tack or peel strengths a polymer must be sufficiently viscoelastic (liquid-like) to enable fibrillation.[35,36] Very recently, Deplace et al.[35] and Creton et al.[36] have shown good analogy between the plateau stress of the probe tack test and the tensile test.

Roberts[32] has proposed that during the bond separation process in the peel test of the autohesive tack joints the strength of the local bonds will be sufficient to cause fibrils to be drawn from the surfaces. Finally, the fibrillar structure will detach from the surface. Glassmaker et al.[37] have suggested that the detachment of the fibrils from the surface of the probe (in probe tack test) is controlled by the strain hardening of the polymer in the fibrils. The more pronounced the strain hardening, the less the fibrils can extend before detaching from the surface of the probe. Here, addition of nanoclay reasonably increases the elastic modulus of the BIMS rubber (see Figure 9), and also the strength of the fibrils of the filled samples is higher when compared to their unfilled counterpart. Consequently, the tack strength of the clay loaded samples is significantly higher in comparison to the neat BIMS rubber.

Furthermore, in order to have a clear estimate on the strength of the interface, the autohesive tack between B−BSEP8 (joint strength between a strip of B and a strip of BSEP8) has been analyzed. It is interesting to note that tack strength of sample B−BSEP8 is higher than tack strength of B−B (joint strength between a strip of B and a strip of B) but significantly lower than the tack strength of BSEP8−BSEP8 (joint strength between a strip of BSEP8 and a strip of BSEP8) (see inset of Figure 6). This confirms that the interface significantly strengthens only if the entangled chains offer greater resistance to separation from both sides across the interface. Also, the contact angle measurements on the unfilled and clay loaded sample surfaces suggest that the addition of sepiolite nanoclay does not alter the surface properties of the neat BIMS rubber (Figure 10). Therefore, it is clear that most of the surface region of the clay loaded samples still remains rubbery, and hence there will be adequate wetting at the interface for the bond formation. Torro-Palau et al. have reported earlier that the addition of sepiolite filler to polyurethane adhesive does not alter the surface properties of the adhesive.[38]

3.3. Dynamic Mechanical Analysis (DMA). *3.3.1. Temperature Sweep Studies.* Figure 11a,b shows the tan δ and log E' plots against temperature for B, BSEP8, and BSEP16. Generally, for most of the polymers, the tan δ peak occurs at the glass transition temperature (T_g) of the polymer. Here, the glass transition temperature (T_g) of the neat BIMS elastomer is located at −21 °C (Figure 11a). The T_g of the BIMS elastomer matrix is almost not altered by the presence of nanofiller (Table 2). However, the height of the tan δ peak diminishes with increasing clay content (Table 2). This is well expected because the formation of nanostructure restricts the molecular motions. It is known that the height of the dynamic transition of a component of a composite apparently reflects the relative quantity of the component itself. The decrease of tan δ peak height is the result of a reduction of the relative quantity of bulk rubber "active" in the dynamic transition. When the clay concentration is high, more number of the rubber chains can interact with the clay, thereby reducing the active free-rubber chain numbers and resulting in the decrease in tan δ peak height.

However, at 25 °C (temperature at which the peel tests are performed), the tan δ peak height of B (neat BIMS rubber) remains unaltered by the addition of nanoclay. For example, the tan δ peak heights of B and BSEP16 at 25 °C are the same

(i.e., 0.20). Therefore, during peeling the clay loaded samples at 25 °C, the extent of fibrillation will not hampered due the presence of nanoclay. But the strength of the fibrils of the clay loaded samples is higher when compared to their unfilled counterpart due to the nanoclay reinforcement. Consequently, the tack strength of the clay loaded samples is higher.

On the other hand, the plateau modulus values of neat BIMS elastomer gradually increases with the concentration of nanoclay (see Figure 11b). There is good correspondence between the increase in modulus of elastomer (seen in the tensile test) and the increase in plateau modulus of elastomer due to the incorporation of nanoclay. The increase in the plateau modulus values by the addition of nanoclay clearly exemplifies the interaction between the nanoclay and the BIMS elastomer, which is the main reason for the increase in the cohesive strength of the BIMS rubber.

3.3.2. Frequency Sweep Studies. Since the behavior at high frequency is related to the behavior at very low temperature, and vice versa, the frequency sweep tests over a long range of temperature (here, it is between −50 and 125 °C) can be used to understand the behavior at extreme temperatures outside the experimental range, using the time−temperature superposition method. Time−temperature superposition has long been used to obtain temperature-independent master curves for polymer systems by shifting values of storage modulus and loss modulus toward the frequency axis. One reference temperature should be chosen (here, it is 25 °C), and the viscoelastic variables of interest [here, storage modulus (E') and loss modulus (E'')] at other temperatures are shifted to the corresponding values at that reference temperature. A horizontal shift factor, a_T, which is a function of temperature, enables to obtain the master curves. Using the Williams−Landel−Ferry (WLF) equation[39]

$$\log a_T = \frac{-C_1(T - T_g)}{C_2 + (T - T_g)} \tag{3}$$

one can relate the shift factor, a_T, to the glass transition temperature, T_g (T_g + 50 °C is considered as the reference temperature) of a polymer and two constants, C_1 and C_2, which have been found to be characteristic of the polymer's molecular structure. Figure 12 shows the log E' vs log frequency master curves of representative samples (B and BSEP16) at a reference temperature of 25 °C. Similar to B, BSEP16 also obeys the time−temperature superposition principle and displays a linear viscoelastic region. As expected, the addition of nanoclay increases the storage modulus over the entire frequency scale range. This again confirms the reinforcing action of nanoclay in the BIMS matrix.

It is essential to note that the storage modulus, E', is time (and frequency) dependent. As the tack measurements are carried out at room temperature, a measurement of E' vs frequency at room temperature and then estimating the plateau modulus, E_n^0, from this analysis will be more appropriate. For this reason, in this work, the E_n^0 values of the unfilled and the filled samples have been calculated from the low-frequency plateau zone (zone corresponding to the room temperature condition) of the DMA frequency sweep master curves (Figure 12). Cooper-White and Mackay[40] have calculated the plateau modulus values of poly(L-lactic acid) polymers having different molecular weights from the measurements of the dynamic moduli against frequency in the

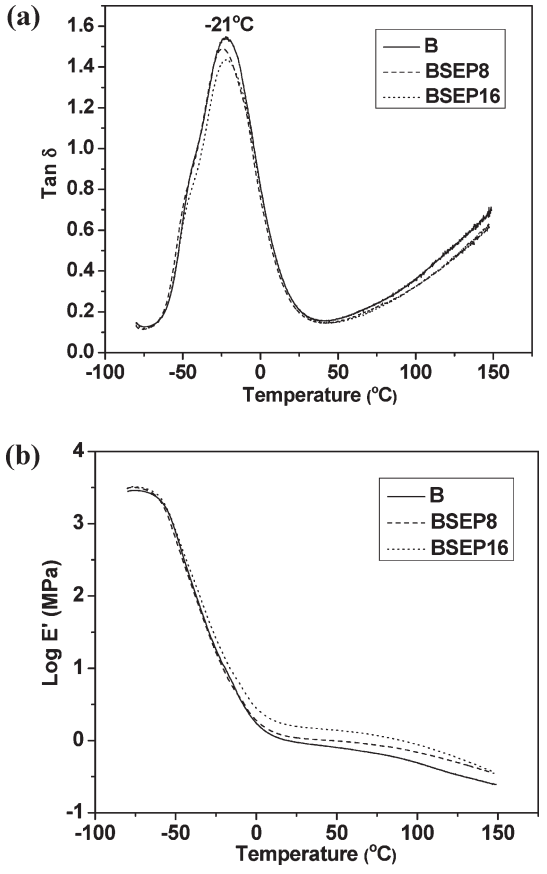

Figure 11. (a) Tan δ vs temperature curves of B, BSEP8, and BSEP16 measured at 1 Hz frequency. (b) Log E' vs temperature curves of B, BSEP8, and BSEP16 measured at 1 Hz frequency.

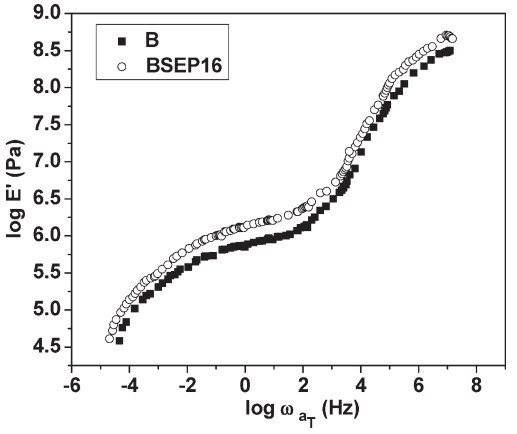

Figure 12. Master curves of log E' vs log reduced frequency at 25 °C for B and BSEP16.

Table 2. Effect of Nanoclay on the Viscoelastic Properties of the BIMS Rubber

sample no.	designation	glass transition temperature, T_g (°C)	tan δ peak height	plateau modulus, E_n^0 (MPa)	entanglement molecular weight, M_e (g/mol)
1	B	−21	1.55	0.79	3117
2	BSEP8	−22	1.48	1.00	2476
3	BSEP16	−21	1.43	1.45	1707

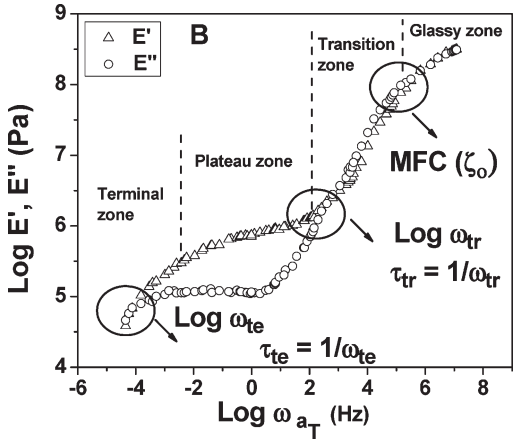

Figure 13. Master curves of log E' and log E'' vs log reduced frequency at 25 °C for B.

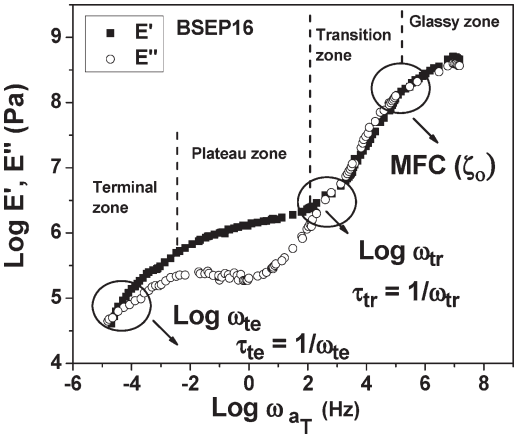

Figure 14. Master curves of log E' and log E'' vs log reduced frequency at 25 °C for BSEP16.

low-frequency zone of the frequency sweep master curves. The plateau modulus, E_n^0, is one of the most important viscoelastic properties that distinguishes entangled polymers from unentangled polymers. Today, it is well-accepted that, once the value of E_n^0 is available, one can determine the molecular weight between entanglement couplings (often referred to as "entanglement molecular weight, M_e"). It is well-known that the self-diffusion of rubber molecules at the tack junction is highly governed by the entanglement density in the plateau zone. The entanglement density in the plateau zone can be accurately estimated from the entanglement molecular weight. The entanglement molecular weight has been estimated from the rubbery plateau modulus using eq 4[39−43]

$$M_e = \frac{\rho RT}{E_n^0} \tag{4}$$

where ρ is the density of the polymer or blend, R is 8.314 J/(mol K), and T is the absolute temperature. The E_n^0 and M_e values of the neat BIMS rubber and the nanocomposites are reported in Table 2. From Table 2, it is observed that the M_e value gradually decreases with increasing nanoclay concentration. This means that the nanoclay has increased the entanglement of the base polymer, and the nanoclay is essentially acting as reinforcing filler in the plateau region. Generally, diluents like oil will significantly reduce the entanglement density of the base polymer and will facilitate the molecular diffusion at the tack junction. However, the diluted interdiffused chains will separate more readily when stressed, and hence the tack strength will be poor.[4,6] On the other hand, properly selected tackifiers will increase the tack strength by simultaneously reducing the entanglement density and by offering greater resistance to separation when stressed.[4,6,8] Here, the addition of nanoclay significantly increases the tack strength of BIMS rubber by increasing the entanglement density of BIMS rubber, which is contrary to the action of oil and tackifier. Therefore, it is conceivable that the strength of the interface strongly depends on the resistance to separation offered by the interdiffused and entangled rubber chains.

Figures 13 and 14 show the logarithmic plots of E' and E'' master curves against frequency for two representative samples (B and BSEP16). These figures clearly illustrate the different zones (terminal, plateau, transition, and glassy zones) of viscoelastic behavior of B and BSEP16, respectively. Several molecular parameters of the polymers and in particular their relaxation times (τ) and monomer friction coefficient (ζ_0) can be identified from the frequency sweep master curve.[44,45] The relaxation times [terminal relaxation time (τ_{te}), onset of transition zone relaxation time (τ_{tr})] and the monomer friction coefficient (ζ_0) have been extracted from the different crossover frequencies (ω_c) where E' and E'' intersect (as shown in Figures 13 and 14).

In the terminal zone, the frequency ω_{te} is roughly the reciprocal of the relaxation time (τ_{te}) required for a molecule to completely rearrange its configuration by snaking itself through numerous entanglements.[43] In the onset of the transition zone, the intersection frequency ω_{tr} is very close to the reciprocal of the relaxation time (τ_{tr}), which is the measure of the time required for complete configurational rearrangement of a piece of macromolecule caught between two cross-links or two entanglements.[43]

In particular, this terminal relaxation time (τ_{te}) corresponds to the reptation time (τ_{rep}), which sets the self-diffusion rate of the rubber molecules at the tack junction.[44,45] Once the reptation time is identified, it is easy to calculate the self-diffusion coefficient (D). Accordingly, at 25 °C, the D values of B, BSEP8, and BSEP16 can be calculated from eq 5[46]

$$\tau_{rep} = \frac{{R_g}^2}{2D} \tag{5}$$

On rearranging the above equation, we get

$$D = \frac{{R_g}^2}{2\tau_{rep}} \tag{6}$$

where R_g is the radius of gyration of BIMS rubber and τ_{rep} is the reptation time.

In addition, the average depth of penetration, Δx, of the BIMS rubber chain can be calculated from the Einstein diffusion equation[47]

$$\langle \Delta x^2(t) \rangle = 2Dt \tag{7}$$

where D is the self-diffusion coefficient and t is the time of contact (here 15 s) during the joining process in the tack test. The monomer friction coefficient (ζ_0) is the average resistance force per monomer unit encountered when a polymer chain moves through its surroundings at a unit speed.[48,49] By assuming that Rouse model describes that high-frequency response of the long chains in the transition zone, we have[48,49]

$$E'(\omega) = E''(\omega) = \rho \nu_0 N_a R_g \sqrt{\frac{\zeta_0 kT\omega}{8 m_0 M}} \tag{8}$$

Table 3. Relaxation Time (τ), Self-Diffusion (D), and Monomer Friction Coefficient (ζ_0) Values of B, BSEP8, and BSEP16

sample no.	designation	τ_{te} (s)	$D \times 10^{-21}$ (m^2/s)	τ_{tr} (s)	log ζ_0 (g/s)
1	B	15 848	9.1	0.002	−1.39
2	BSEP8	25 142	5.7	0.003	−0.52
3	BSEP16	38 018	3.8	0.003	0.37

where $E'(\omega)$ and $E''(\omega)$ are the storage and loss modulus, ω is the frequency, ρ is the density, N_a is Avogadro's number, v_0 is the volume fraction of the base polymer, R_g is the radius of gyration, k is the Boltzmann constant, T is the absolute temperature, m_0 is the monomer molecular weight, and M is the molecular weight of the base polymer. For BIMS rubber, the R_g value has been taken from the literature.[50] The monomer friction coefficient (ζ_0) value has been calculated using eq 8.

The important molecular or rheological parameters such as relaxation times (τ), monomer friction coefficient (ζ_0), and self-diffusion coefficient (D) of B, BSEP8, and BSEP16 have been extracted from the frequency sweep master curves, and their values are listed in Table 3. From the third column of Table 3, it is evident that the terminal relaxation time (τ_{te}) of the neat BIMS rubber increases with the addition of nanoclay. In the clay loaded samples, the rubber chains contours will be extensively intermingled, so each chain is surrounded all along its length by a mesh of neighboring chain contours. Rearrangement on a large scale is retarded because the chain cannot cross through its neighbors, and hence the terminal relaxation time (τ_{te}) increases.

The self-diffusion coefficient (D) values calculated from eq 6 for sample B, BSEP8, and BSEP16 are reported in the fourth column of Table 3. The D value of sample B has been estimated as 9.1×10^{-21} m^2/s. This value can be compared with the previously reported value. Ellul and Gent found the D value of polyisobutylene (PIB) rubber to be 2×10^{-21} m^2/s at 25 °C, which was estimated using the well-known Bueche's relation.[51] From Table 3, it is seen that the self-diffusion value of BIMS rubber decreases with the addition of nanoclay, which is ascribed to the restriction in molecular mobility [longer terminal relaxation time (τ_{te})] across the interface due to the nanoclay reinforcement. Furthermore, the average depth of penetration calculated as $\langle \Delta X^2(t) \rangle = 2Dt$; i.e., a distance that the BIMS chain diffuses at 15 s contact time is 0.52 nm, which is lower than the radius of gyration of the BIMS rubber coil (17 nm). The average penetration depth of the samples BSEP8 and BSEP16 is 0.41 and 0.34 nm, respectively. This again suggests the same that the reinforcing effect of nanoclay reduces the average penetration depth of the rubber chain across the interface.

It is well-known that in order to "heal" the interface (i.e., the interface achieves the cohesive strength) between the rubbers, chains only need to diffuse a distance on the order of the radius of gyration of the chains.[52] Here, in the case of neat BIMS rubber, we have estimated that the rubber chain diffuse 0.52 nm during 15 s contact time, which is lower than the radius of gyration of BIMS rubber coil (17 nm), and hence the rubber strips (B−B) could be easily separated during the peel test. On the other hand, in the case of sample BSEP16, it has been estimated that the rubber chain can diffuse only 0.34 nm during 15 s contact time, which is lower that the ΔX value of sample B. But, interestingly the rubber strips (BSEP16−BSEP16) could not be separated during the peel test. From the above data, it is for sure that the interface of the clay loaded samples cannot achieve cohesive strength during 15 s contact time. Therefore, the difficulty in separating the rubber strips (BSEP16−BSEP16) can only be correlated to the existence of more restrictions for the diffused rubber chains to separate because of the higher monomer friction coefficient (ζ_0) in the interface of the nanocomposite samples due to the nanoclay reinforcement.

From the fifth column of Table 3, it is seen that the relaxation time (τ_{tr}) of the neat BIMS rubber only marginally increases with the addition of nanoclay. This suggests the existence of slightly higher restrictions for a single BIMS rubber molecule to relax due to the constraints imposed by nanoclay particles. Finally, from the sixth column of Table 3, it is observed that the monomer friction coefficient (ζ_0) value increases with the addition of the nanoclay. The possible reason for the increment of the monomer friction coefficient value (ζ_0) by the addition of nanoclay can be due to the reinforcing action of the nanoclay in the BIMS matrix, which will restrict the segmental mobility. Furthermore, it is clear from Figure 11a that the addition of the nanoclay causes a reduction in the height of the tan δ peak which is due restrictions imposed on molecular motions by the nanoclay.

From the terminal relaxation time and self-diffusion coefficient values, it is clear that the flow and chain interdiffusion across the interface are lower for the clay loaded sample in comparison with the neat BIMS rubber. Although BSEP8 and BSEP16 register lower self-diffusion coefficient value than B, the tack strengths of BSEP8 and BSEP16 are significantly higher than the tack strength of B. Hence, for a given extent of self-diffusion, we have to analyze if there is a difference in the resistance to separation in between the unfilled and the clay loaded samples. Here, the greater bond breaking resistance of nanocomposites is well justified by the higher onset of transition zone relaxation time (τ_{tr}) and monomer friction coefficient (ζ_0) values of BSEP8 and BSEP16 in comparison with sample B. Therefore, it may be derived that even at 16 phr loading of nanoclay, the increase in transition zone relaxation time (τ_{tr}) and monomer friction coefficient (ζ_0) values dominates over the decrease in the self-diffusion coefficient value. The drop in self-diffusion coefficient value is sufficiently low that it does not affect the bond formation ability (entanglement formation ability) of the rubber chains across the interface, and hence tack strength prominently increases by the addition of nanoclay.

4. Conclusions

The influence of needle-like sepiolite nanoclay on the autohesive tack (self-diffusion) behavior of brominated isobutylene-*co*-*p*-methylstyrene (BIMS) rubber has been investigated here in the context of various autohesive tack governing factors such as relaxation times (τ), self-diffusion coefficient (D), monomer friction coefficient (ζ_0), and average penetration depth of rubber chains (Δx) across the interface. The use of nanoclay as a filler in BIMS rubber leads to a significant increase in the autohesive tack strength of BIMS rubber. For instance, the tack strength of 2 and 8 phr of nanoclay loaded BIMS rubber is approximately 140% and 300% higher than the tack strength of the unfilled BIMS rubber. The needle-shaped sepiolite nanoclay is found to be well dispersed in the BIMS rubber matrix as evidenced from the XRD spectra, AFM images, and TEM micrographs of the nanocomposites. In the tensile stress−strain curves, incorporation of nanoclay increases the elastic modulus of the BIMS rubber, and also the strength of the fibrils formed during the separation process of the clay loaded samples is higher when compared to their unfilled counterpart. This phenomenon significantly contributes to the enhancement of the tack strength.

The incorporation of nanoclay reduces self-diffusion coefficient (D) of BIMS rubber (by increasing the terminal relaxation time, τ_{te}) due to the reinforcing action of the nanoclay. However, the average penetration depth of rubber chains (Δx) across the interface in the clay loaded samples is still sufficient to establish

entanglements on either side of the interface and the entangled chains offer more resistance to separation upon stressing due to the existence of higher monomer friction coefficient (ζ_0) and onset of transition zone relaxation time (τ_{tr}) in the nanoclay loaded samples when compared to the unfilled sample. Consequently, the tack strengths of the clay loaded samples are markedly higher than the unfilled sample.

Acknowledgment. The authors are thankful to The Exxon-Mobil Chemical Co., USA for sponsoring the project and granting permission to publish the results.

References and Notes

(1) Aradian, A.; Raphael, E.; de Gennes, P.-G. *Macromolecules* **2000**, *33*, 9444–9451.
(2) Kim, Y. H.; Wool, R. P. *Macromolecules* **1983**, *16*, 1115–1120.
(3) Voyutskii, S. S. *Autohesion & Adhesion of High Polymers*; Interscience Publishers: New York, 1963; Chapters 1 and 2, pp 5−59.
(4) Hamed, G. R. *Rubber Chem. Technol.* **1981**, *54*, 576–595.
(5) Rhee, C. K.; Andries, J. C. *Rubber Chem. Technol.* **1981**, *54*, 101–114.
(6) Hamed, G. R.; Roberts, G. D. *J. Adhes.* **1994**, *47*, 95–113.
(7) Bhowmick, A. K.; De, P. P.; Bhattacharyya, A. K. *Polym. Eng. Sci.* **1987**, *27*, 1195–1202.
(8) Kumar, K. D.; Tsou, A. H.; Bhowmick, A. K. *J. Adhes. Sci. Technol.* **2008**, *22*, 2039–2058.
(9) Beatty, J. R. *Rubber Chem. Technol.* **1969**, *42*, 1040–1053.
(10) Busse, W. F.; Lambert, J. M.; Verdery, R. B. *J. Appl. Phys.* **1946**, *17*, 376–385.
(11) Beckwith, R. K.; Welch, L. M.; Nelson, J. F.; Chaney, A. L.; McCracken, E. A. *Rubber Chem. Technol.* **1950**, *23*, 933–944.
(12) Kumar, B.; De, P. P.; De, S. K.; Peiffer, D. G.; Bhowmick, A. K. *J. Adhes. Sci. Technol.* **2001**, *15*, 1145–1163.
(13) Bhaumik, T. K.; Gupta, B. R.; Bhowmick, A. K. *J. Adhes. Sci. Technol.* **1987**, *1*, 227–238.
(14) Vaia, R. A.; Lincoln, D. In *Polymer Nanocomposites: Synthesis, Characterization and Modeling*; Krishnamoorti, R., Vaia, R. A., Eds.; ACS Symposium Series No. 804; American Chemical Society: Washington, DC, 2000; Chapter 9, p 102.
(15) Ray, S. S.; Okamoto, M. *Prog. Polym. Sci.* **2003**, *28*, 1539–1641.
(16) Maiti, M.; Bhattacharya, M.; Bhowmick, A. K. *Rubber Chem. Technol.* **2008**, *81*, 384–469.
(17) Sadhu, S.; Bhowmick, A. K. *J. Polym. Sci., Part B: Polym. Phys.* **2004**, *42*, 1573–1585.
(18) Maiti, M.; Bhowmick, A. K. *J. Polym. Sci., Part B: Polym. Phys.* **2006**, *44*, 162–176.
(19) Maiti, M.; Bhowmick, A. K. *Compos. Sci. Technol.* **2008**, *68*, 1–9.
(20) Bhattacharya, M.; Bhowmick, A. K. *Polymer* **2008**, *49*, 4808–4818.
(21) Bhattacharya, M.; Maiti, M.; Bhowmick, A. K. *Polym. Eng. Sci.* **2009**, *49*, 81–98.
(22) Choudhury, A.; Bhowmick, A. K.; Ong, C. *Polymer* **2009**, *50*, 201–210.
(23) Bilotti, E.; Fischer, H. R.; Peijs, T. *J. Appl. Polym. Sci.* **2008**, *107*, 1116–1123.
(24) Krishnan, R.; Mackay, M. E.; Duxbury, P. M.; Pastor, A.; Hawker, C. J.; Van Horn, B.; Asokan, S.; Wong, M. S. *Nano Lett.* **2007**, *7*, 484–489.
(25) Balazs, A. C. *Nat. Mater.* **2007**, *6*, 94–95.
(26) Patel, S.; Bandyopadhyay, A.; Ganguly, A.; Bhowmick, A. K. *J. Adhes. Sci. Technol.* **2006**, *20*, 371–385.
(27) Li, H.; Yang, Y.; Yu, Y. *J. Adhes. Sci. Technol.* **2004**, *18*, 1759–1770.
(28) Wang, T.; Colver, P. J.; Bon, S. A. F.; Keddie, J. L. *Soft Matter.* **2009**, *5*, 3842–3849.
(29) Chang, R.-J.; Gent, A. N. *J. Polym. Sci., Part B: Polym. Phys.* **1981**, *19*, 1619–1633.
(30) Zosel, A. *Colloid Polym. Sci.* **1985**, *263*, 541–553.
(31) Duquesne, E.; Moins, S.; Alexandre, M.; Dubois, P. *Macromol. Chem. Phys.* **2007**, *208*, 2542–2550.
(32) Roberts, G. D. Ph.D. Thesis, University of Akron, **1991**.
(33) Roe, R. J.; Davis, D. D.; Kwei, T. K. *Bull. Am. Phys. Soc.* **1970**, *15*, 308.
(34) Prager, S.; Tirrell, M. *J. Chem. Phys.* **1981**, *75*, 5194–5198.
(35) Deplace, F.; Carelli, C.; Mariot, S.; Retsos, H.; Chateauminois, A.; Okzineb, K.; Creton, C. *J. Adhes.* **2009**, *85*, 18–54.
(36) Creton, C.; Hu, G.; Deplace, F.; Morgret, L.; Shull, K. R. *Macromolecules* **2009**, *42*, 7605–7615.
(37) Glassmaker, N. J.; Hui, C. Y.; Yamaguchi, T.; Creton, C. *Eur. Phys. J. E* **2008**, *25*, 253–266.
(38) Torro-Palau, A.; Fernandez-Garcia, J. C.; Orgiles-Barcelo, A. C.; Pastor-Blas, M. M.; Martin-Martinez, J. M. *J. Adhes. Sci. Technol.* **1997**, *11*, 247–262.
(39) Ferry, J. D. *Viscoelastic Properties of Polymers*, 3rd ed.; Wiley: New York, 1982; Chapter 13, pp 366−403.
(40) Cooper-White, J. J.; Mackay, M. E. *J. Polym. Sci., Part B: Polym. Phys.* **1999**, *37*, 1803–1814.
(41) Tobing, S. D.; Klein, A. *J. Appl. Polym. Sci.* **2000**, *76*, 1965–1976.
(42) Yuan, B.; McGlinchey, C.; Pearce, E. M. *J. Appl. Polym. Sci.* **2006**, *99*, 2408–2413.
(43) Ferry, J. D.; Kramer, O. In *Science and Technology of Rubber*; Eirich, F. R., Ed.; Academic Press: New York, 1978; Chapter 5, pp 179−221.
(44) Schach, R.; Creton, C. *J. Rheol.* **2008**, *52*, 749–767.
(45) Schach, R.; Tran, Y.; Menelle, A.; Creton, C. *Macromolecules* **2007**, *40*, 6325–6332.
(46) Roland, C. M.; Boehm, G. *Macromolecules* **1985**, *18*, 1310–1314.
(47) Jud, K.; Kausch, H. H.; Williams, J. G. *J. Mater. Sci.* **1981**, *16*, 204–210.
(48) Colby, R. H.; Fetters, L. J.; Graessley, W. W. *Macromolecules* **1987**, *20*, 2226–2237.
(49) Tse, M. F. *J. Adhes. Sci. Technol.* **1989**, *3*, 551–570.
(50) Kumar, K. D.; Gupta, S.; Tsou., A. H.; Bhowmick, A. K. *J. Appl. Polym. Sci.* **2008**, *110*, 1485–1497.
(51) Ellul, M. D.; Gent, A. N. *J. Polym. Sci., Part B: Polym. Phys.* **1984**, *22*, 1953–1968.
(52) Qureshi, N. Z.; Stepanov, E. V.; Capaccio, G.; Hiltner, A.; Baer, E. *Macromolecules* **2001**, *34*, 1358–1364.